Uncertainty Estimates of the EOF-Derived North Atlantic Oscillation

YI-HUI WANG AND GUDRUN MAGNUSDOTTIR

Department of Earth System Science, University of California, Irvine, Irvine, California

HAL STERN, XU TIAN, AND YAMING YU

Department of Statistics, University of California, Irvine, Irvine, California

(Manuscript received 13 April 2013, in final form 20 August 2013)

ABSTRACT

Different approaches to obtaining uncertainty estimates of the North Atlantic Oscillation (NAO) are explored. The resulting estimates are used to enhance the understanding of spatial variability of the NAO over different time periods. Among the parametric and nonparametric approaches investigated in this study, the bootstrap is nonparametric and not confined to the assumption of normally distributed data. It gives physically plausible uncertainty estimates. The NAO uncertainty estimates depend on sample sizes with greater sampling variability as sample size is smaller. The NAO uncertainty varies with time but common features include that the most uncertain values are centered between the centers of action of the NAO and are asymmetric in the zonal direction (more uncertainty in the eastward direction or downstream). The bootstrap can also be used to provide direct measures of uncertainty regarding the location of the NAO action centers. The uncertainty of the location of the NAO action centers not only helps assess the shift in the NAO but also provides evidence of more than two action centers. The methods reported on here could in principle be applied to any EOF-derived climate pattern.

1. Introduction

Empirical orthogonal function (EOF) analysis is widely used in the climate community to define large-scale climate patterns. EOF analysis provides the eigenvectors and eigenvalues of the spatial covariance matrix of a meteorological field, thereby characterizing the spatial patterns of atmospheric and oceanic variability, which organize coherent variations over large regions (for a review see, e.g., Hannachi et al. 2007). For instance, the wintertime North Atlantic Oscillation (NAO) is frequently defined as the leading EOF mode of sea level pressure (SLP) over the North Atlantic and surrounding continents. The temporal variability of this spatial pattern is measured by the NAO index, which is obtained by projecting the spatiotemporal data onto the EOF-defined NAO pattern. The NAO has also been defined and measured by normalized SLP at two fixed stations (Stykkisholmur and Azores, Hurrell 1995), one-point correlation maps (Wallace and Gutzler 1981), and cluster analysis (Cassou et al. 2004). These methods generate similar NAO patterns. Since the NAO is most often defined by EOF analysis, our results are based on the EOF-derived NAO.

Conventionally, the NAO is viewed as a stationary spatial pattern of variability over a time period. Recent studies have indicated that the NAO is nonstationary on decadal time scales. The pronounced nonstationarity of the NAO patterns was first noticed when the northern center of action of the NAO shifted eastward during the winters 1978–97 compared to 1958–77 (e.g., Hilmer and Jung 2000; Wang and Magnusdottir 2012). Zhang et al. (2008) applied EOF analysis to data over the Northern Hemisphere and found a shift in the centers of action of the northern annular mode in the early 2000s (analogous to the NAO, except the domain covers the entire Northern Hemisphere north of 20°N) using 5-yr running windows over 1958/59–2006/07. Wang et al. (2012) discovered and quantified the movement of the NAO in 20-yr sliding windows over 1871–2008. They not only confirm the eastward movement of the northern center of action of the NAO during the winters of 1978–97 but also point out the eastward shift of the southern center

Corresponding author address: Gudrun Magnusdottir, Department of Earth System Science, University of California, Irvine, Irvine, CA 92697-3100.
E-mail: gudrun@uci.edu

DOI: 10.1175/JCLI-D-13-00230.1

of action during the late nineteenth century and mid-twentieth century.

The nonstationary NAO behavior in different sliding windows points to a limitation of EOF analysis. EOF analysis is not usually accompanied by a measure of the uncertainty associated with the identified pattern. Because of the absence of an uncertainty measure, researchers may be unaware of the influence of sampling variability on EOF due to, for example, short records of data. Furthermore, uncertainty estimates of the NAO may lead to physical intuition regarding the NAO spatial variability. For instance, uncertainty estimates could help calibrate the significance of the decadal shifts in the NAO. A few studies have estimated the sampling variability in eigenvectors using asymptotic methods (North et al. 1982; Quadrelli et al. 2005), but they did not focus on sampling variability of the NAO and its implication for spatial variability of the NAO. One of the main goals of this study is to compare different approaches for obtaining NAO uncertainty estimates. Investigating the implication of NAO uncertainty for climate statistics is another objective. We believe that NAO uncertainty not only provides an intuitive presentation of NAO spatial variability but also helps assess the robustness of the movement of the centers of action of the NAO.

In this study, we will carry out both the asymptotic approximation and bootstrap techniques, illustrated in sections 2b and 2c, to measure NAO uncertainty in space based on wintertime monthly data. The measures of NAO uncertainty estimated by these methods are compared in sections 3a and 3b. We will address the relative impact of sampling variability on NAO uncertainty using different lengths of data in section 3c. We will show the characteristics of the NAO uncertainty from both statistical and physical perspectives in section 3d. We will also discuss the implication of the distribution of the occurrences of NAO action centers obtained by the bootstrap technique in section 3e. The summary and discussion are included in the last section.

2. Data and methods

a. Data

This study uses monthly SLP in winter (December–March) during 1871–2008 from the second version of Twentieth Century Reanalysis (20CRv2), which has a spatial resolution 2° latitude × 2° longitude (Compo et al. 2011). Monthly anomalies of a variable are obtained by subtracting the monthly mean over a time period of interest from the relevant month. Prior to EOF analysis, we weigh the SLP anomalies by the square root cosine of latitude to ensure that data points near the pole do not have a disproportionate impact on the analysis. The NAO uncertainty estimates of different periods are derived using a number of approaches including a parametric method, the asymptotic approximation, and two nonparametric methods: the ordinary bootstrap and the nonoverlapping block bootstrap.

b. Asymptotic approximation

In statistics, asymptotic approximations provide a distribution for a statistic (e.g., an eigenvector) that is valid for large sample sizes. It is common to work with the probability distribution of EOFs based on the assumption that the original data follow a multivariate normal distribution (Jolliffe 2002). The standard deviation of eigenvalues and eigenvectors can then be approximated by the asymptotic formula (Seber 1984).

The uncertainty associated with the kth eigenvector t_k is measured by the variance matrix $\mathbf{D}$, a square matrix with dimension equal to the number of spatial locations. The vector of standard deviations of t_k at the different locations is obtained as the square roots of the diagonal elements of the matrix $\mathbf{D}$,

$$\mathbf{D} = \frac{1}{n} \sum_{j \neq k} l_k l_j (l_k - l_j)^{-2} \mathbf{t}_j \mathbf{t}_j'.$$

The above equation shows that the standard deviation of t_k is determined by other nonzero eigenvalues l_j and eigenvectors $\mathbf{t}_j$; $\mathbf{t}_j'$ is the transpose of $\mathbf{t}_j$. The n represents the sample size. The North rule of thumb (North et al. 1982) uses this result but only uses a single term in the summation. We use multiple terms in the sum to get more precise estimates, though we still eliminate the insignificant contributions associated with small eigenvalues. The standard deviation of the NAO (t_1) is estimated in this work using only the following nine eigenvalues and eigenvectors, which are from the 2nd to the 10th modes. Even though the asymptotic approximation provides the variability of EOF analysis, its validity may be questioned for three reasons. First, the data may not be normally distributed. Second, the sample size may not be large enough. Third, the time series of climate data are generally somewhat autocorrelated. We will address these limitations below.

c. Ordinary bootstrap and nonoverlapping block bootstrap

The ordinary bootstrap addresses two of the three limitations of uncertainty estimates by the asymptotic approximation. The nonoverlapping block bootstrap, introduced below, addresses the third limitation associated with possible autocorrelation in the data. In general, the bootstrap can estimate the uncertainty of EOFs without the constraint of a theoretical distribution

(Efron and Tibshirani 1994). It can also provide informative uncertainty estimates no matter what the size of the dataset.

The bootstrap is a resampling technique in which replicate datasets are constructed through repeated resampling of the original dataset. The relationship of the replicate data to the observed data is the same as the relationship of the observed data to the underlying population. Therefore, the replicate datasets can be used to provide accurate information about our estimated EOF. The bootstrap uses the concept of a Monte Carlo algorithm to sample data from the observed data. Monte Carlo simulations have been applied to assessing the statistical significance of eigenvalues (e.g., Peng and Fyfe 1996; Venegas et al. 1997). However, no climate study (to our knowledge) has quantified the variability of eigenvectors by bootstrapping.

From each replicate dataset, composed of independent data from the original dataset with the same data size (von Storch and Zwiers 1999), we can compute a statistic. A statistic can apply to any of the different variables of interest. In this study, the statistic is the first eigenvector of the covariance matrix. After repeated sampling for a large number of times, the empirical distribution of a statistic is formed. The standard deviation derived from the empirical distribution indicates its variability.

We will apply this concept of the bootstrap to estimate the NAO uncertainty. Initially, we display the spatiotemporal atmospheric field, that is, SLP anomaly, as a matrix **F**. Each row of **F** shows the map of SLP anomaly at a certain time and each column of **F** represents a time series for one grid point. Because our statistic of interest is the first eigenvector of the covariance matrix, a new spatiotemporal data matrix is generated by resampling the time ordering of each location from the observational data matrix. Each time point has equal possibility to be chosen, which means that some members of rows in **F** may appear many times in the new matrix while others may not appear at all. The diagram of the original data matrix and an example of a replicate data matrix in an ordinary bootstrapping process are shown in Fig. 1a.

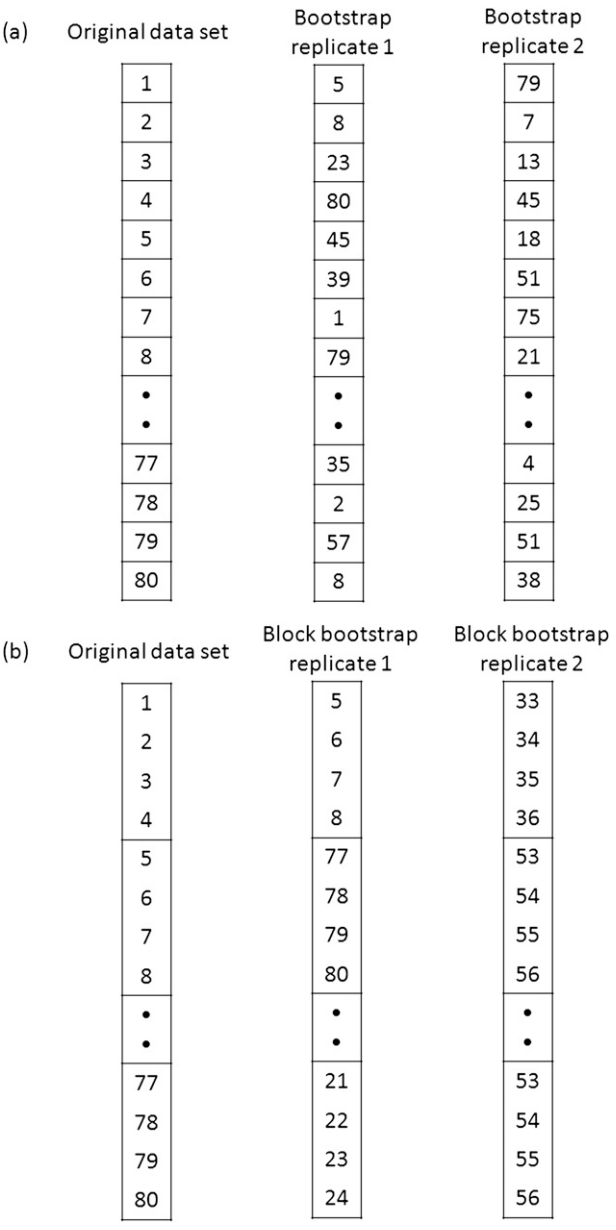

FIG. 1. Diagram depicting the original dataset (numbered by month in the time series) and replicate datasets after random resampling (a) for the ordinary bootstrap and (b) for the nonoverlapping block bootstrap where each box shows one time block.

The EOF1s from the set of bootstrapped covariance matrices constitute an empirical distribution of the EOF from which we can measure the uncertainty by its standard deviation. An empirical distribution of the occurrences of NAO action centers, or nodes, is also provided by the bootstrap technique. We can examine the distribution of the locations of each node to assess spatial uncertainty about the center. Note that we fix the sign of each bootstrap member so that the northern node is always negative. Usually, 200 bootstrap replications can estimate a standard error very close to that by infinite resampling (Efron and Tibshirani 1994). To ensure that we have an accurate approximation, 1000 replications are used in our analyses.

The ordinary bootstrap may not be capable of accurately capturing the sample distribution of a statistic when the underlying data exhibit temporal dependence [von Storch and Zwiers (1999), third limitation in section 2b], which often occurs in climate data.

Theoretically, computing variances of statistics (e.g., the sample mean) derived from dependent data using the usual variance estimator tends to underestimate the true variability of the statistic because the dependence is not accounted for in the formula. The ordinary bootstrap may fail because in its resampling it does not replicate the correlation structure of the original data and, thus, variability of the statistic among the bootstrap samples may remain an underestimate. Alternatively, the block bootstrap tries to replicate the correlation structure in each sample by sampling blocks of data instead of individual observations (see, e.g., Kunsch 1989). Blocks represent sets of continuous data of fixed length (Wilks 1997). Ideally, if the block length can properly accommodate the time dependence (memory) of data, the uncertainty estimates by the block bootstrap would be greater than by the ordinary bootstrap. However, it can be challenging to determine the accurate block length.

The procedure of the block bootstrap is almost the same as the ordinary bootstrap except, instead of drawing monthly data when obtaining a bootstrap sample, we draw blocks of monthly data. The nonoverlapping block bootstrap extracts nonoverlapping blocks from the original data. If data have a record of length n, $\{X_1, X_2, \ldots, X_n\}$, and block length l, the first block of data is $\{X_j: j = 1, \ldots, l\}$, the second block, which has to follow the first one, is $\{X_{l+j}: j = 1, \ldots, l\}$, and this process continues (Gentle et al. 2004). To summarize, n/l number of blocks can be chosen from the original data in the nonoverlapping block bootstrap. Decadal variability of the NAO is difficult to represent by the nonoverlapping block bootstrap because there are too few time blocks in 20-yr data and this would lead to very small values of NAO uncertainty. In this study, we mainly apply the nonoverlapping block bootstrap to 20-yr wintertime monthly data and assume that data are dependent in the same winter. The block sizes that we have examined are two months and four months (one winter). Thus, n is 80 months and l is 2 months [i.e., December–January (DJ) or February–March (FM)] or 4 months [i.e., December–March (DJFM)] for a 20-yr time window. The diagram of the original data matrix and an example of a replicate data matrix in a nonoverlapping block bootstrapping process are shown in Fig. 1b. We will compare the standard deviation of the NAO by the nonoverlapping block bootstrap to the estimate by the ordinary bootstrap. The comparison will shed some light on the effectiveness of the 2-month and 4-month blocks of NAO uncertainty. For brevity, the NAO uncertainty estimated by the 2-month block bootstrap is not shown because of its similarity to the spatial pattern of the NAO uncertainty estimated by the 4-month block bootstrap. To avoid confusion about terminology, we use the term "bootstrap" to refer to the ordinary bootstrap and "block bootstrap" to refer to the nonoverlapping block bootstrap in the following.

3. Results

This study estimates the NAO uncertainty in terms of pointwise standard deviation over the North Atlantic (20°–80°N, 90°W–40°E) by applying the aforementioned methods to different lengths of data. We are interested in understanding the relationship of the NAO uncertainty estimates and displacement/movement of the NAO action centers between the two 20-yr winter periods 1958–77 and 1978–97. There was a well-documented eastward shift in the northern center of action of the NAO from the earlier to the later period (e.g., Hilmer and Jung 2000). In line with Wang et al. (2012), in addition to these two 20-yr periods, other 20-yr running windows are used to get a big picture of the temporal variability of NAO uncertainty estimates.

a. Comparison of uncertainty estimates between the asymptotic approximation and the bootstrap

To assess the performance of different approaches in estimating uncertainty of the NAO in winter, we focus here on the two 20-winter periods of 1958–77 and 1978–97. These two 20-yr periods have noticeably different NAOs as seen comparing the contours in Fig. 2a to those in Fig. 2d. The color shading in Fig. 2 shows the standard deviation of the NAO, evaluated using different methods. Figure 3 shows the identical field except scaled by the maximum value in each panel. The difference in the magnitude of standard deviation between the two periods is shown in Fig. 2 while the difference in its spatial pattern is highlighted in Fig. 3. Although the spatial pattern of standard deviation is similar between the asymptotic approximation and the bootstrap techniques in each period (Fig. 3), the magnitude based on the asymptotic approximation is noticeably smaller than that of the bootstrap and the block bootstrap (Fig. 2). It is difficult to determine whether the pointwise NAO value (the value of the NAO pattern at each grid point, hereafter the NAO coefficient) is normally distributed or whether the sample size of 80 months of data (4 winter months over 20 years) is large enough for the asymptotic approximation. The bootstrap technique is not restricted by the requirement of normally distributed data. Since the NAO uncertainty estimates based on the asymptotic approximation and the bootstrap show better agreement as the sample size increases (not shown), we conclude that the bootstrap technique provides a better representation of uncertainty estimates for the 20-yr windows.

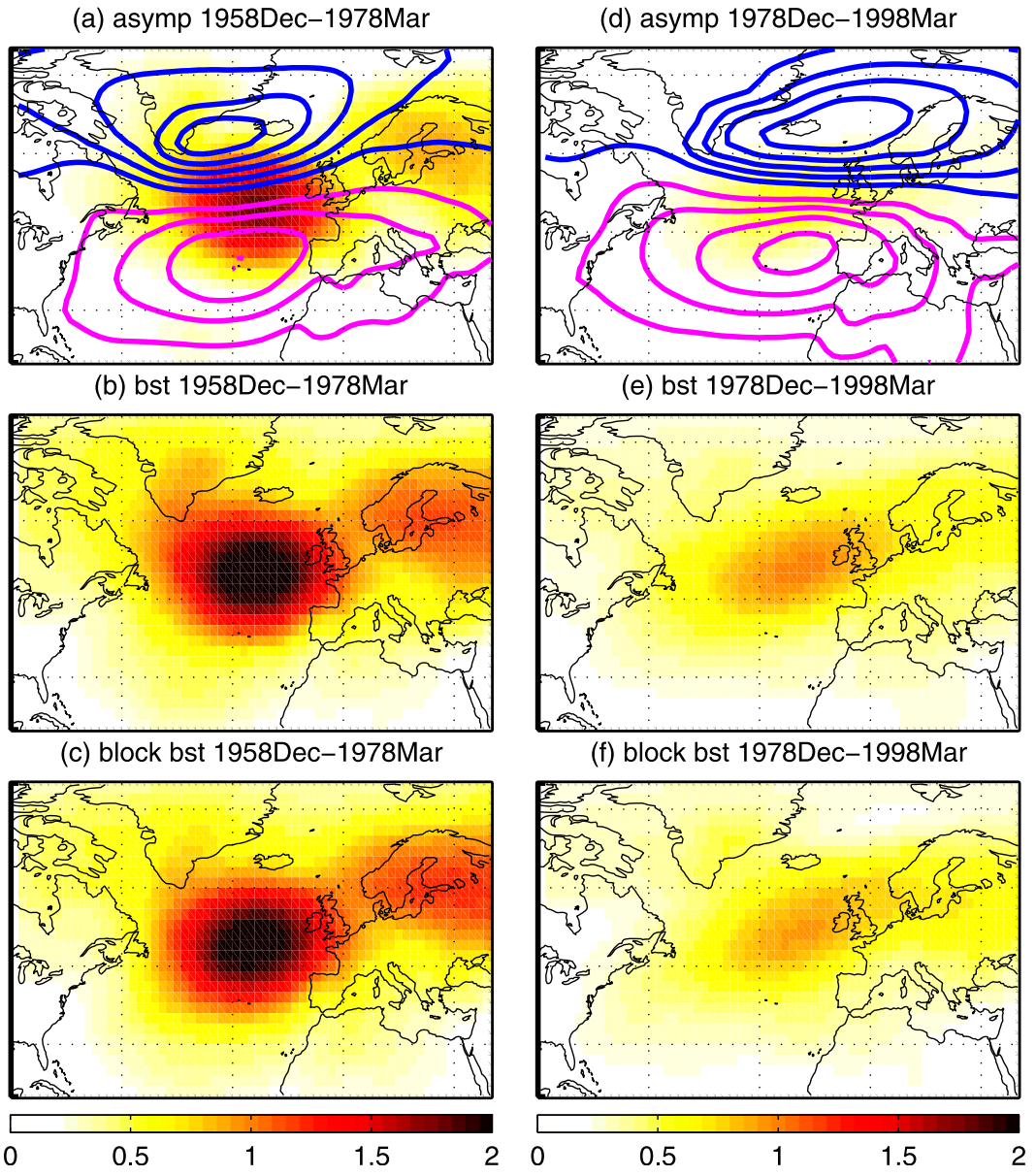

FIG. 2. Standard deviation of the NAO derived from (top) the asymptotic approach, (middle) the bootstrap, and (bottom) the block bootstrap without any scaling. NAO patterns are derived from the regression of SLP anomalies onto the normalized NAO index (contours). Positive values are in magenta, negative values are in blue, the contour interval is 1 hPa, and the zero contour is omitted. The results are from the winters of (left) December 1958–March 1978 and (right) December 1978–March 1998.

b. *Comparison of uncertainty estimates between the bootstrap and the block bootstrap*

The bootstrap breaks the chronological structure in observations, thereby underestimating the variability among different time blocks. In other words, the standard deviation of the NAO for each time period may be larger if the time dependence of data is correctly accounted for. The standard deviation of the NAO by the block bootstrap should be higher than that from the bootstrap if there is a need to account for time dependence and if the block sizes used in this study are accurate depictions of the time dependence.

To better interpret the difference in uncertainty estimates between the bootstrap techniques, the difference in standard deviation between the block bootstrap and the bootstrap for these two 20-yr periods is shown in Fig. 4. The block size of the block bootstrap in Figs. 4a,b is 4 months and that in Figs. 4c,d is 2 months. For the areas with large standard deviation (which are the ones of

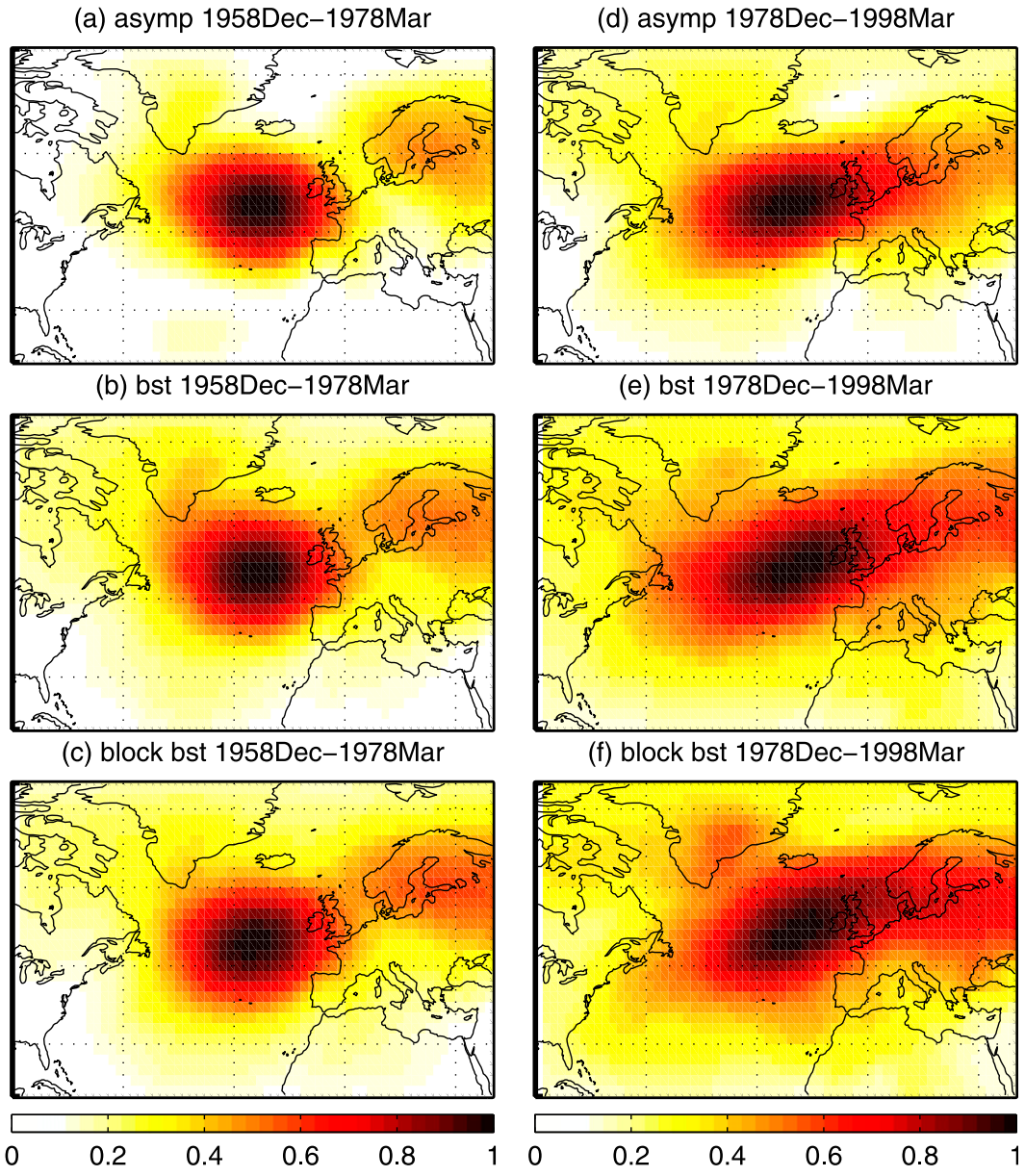

FIG. 3. As in Fig. 2, but the standard deviation of the NAO is scaled by the maximum value of each panel.

most interest), the differences between the block bootstrap and the bootstrap are relatively small (values are approximately 10% of the magnitude of large standard deviation). Compared to the difference in NAO uncertainty between the 4-month block bootstrap and the bootstrap, the difference between the 2-month block bootstrap and the bootstrap is small over most regions of the North Atlantic sector for both 20-yr periods. The greater value of the standard deviation of the NAO coefficients by the block bootstrap compared to the bootstrap is not detected everywhere. The result implies that the time dependence of data is probably not an important factor in the uncertainty estimates. This statement is supported by the autocorrelation of the monthly NAO index in winter, which is derived from projecting time–space SLP anomalies onto the NAO of each 20-yr period. The autocorrelation of the monthly NAO index in winter of both 20-yr periods drops to 0.24 for 1958–77 and 0.34 for 1978–97 at 1-month lag. The autocorrelation drops to lower than 0.2 and becomes insignificant at larger lags. Since the 2-month and 4-month block bootstraps are not helpful to improve the interpretation of the NAO uncertainty, henceforth we use the bootstrap as the main measurement of standard deviation.

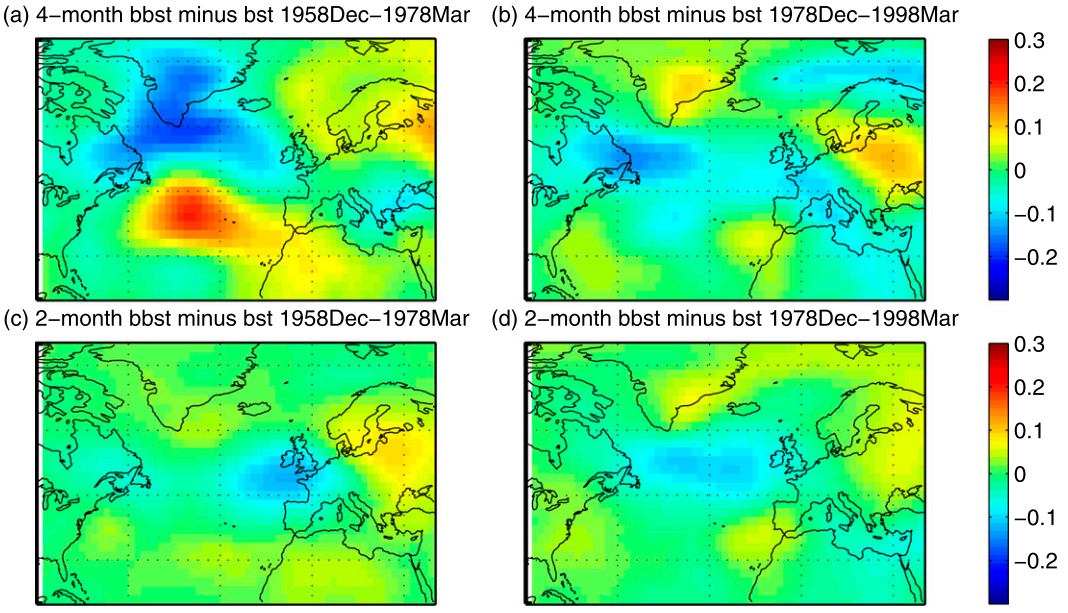

FIG. 4. The difference in standard deviation between the block bootstrap with two different block sizes and the (ordinary) bootstrap during DJFM for 20-yr periods. The block sizes are (top) 4 months and (bottom) 2 months. The results are from the winters of (left) December 1958–March 1978 and (right) December 1978–March 1998.

c. *The effect of different lengths of data on NAO uncertainty estimates*

Investigating the influence of sample size on the NAO uncertainty is one objective of this study. Figure 5 shows the NAO (contours) and its corresponding standard deviation (shading) by the bootstrap for different lengths of data. Figure 5a shows the 5-yr window centered on 1987. The year 1987 is the 5th year of the 10-yr time period (Fig. 5b) and the 10th year of the 20-yr time period (Fig. 5c). All of the NAO patterns in these three periods resemble the long-term NAO, which has two anticorrelated centers of action in the North Atlantic sector. However, as expected, the 5-yr interval (Fig. 5a) has the largest pointwise standard deviation, followed by the 10-yr (Fig. 5b) and 20-yr intervals (Fig. 5c). The maximum standard deviation for the 5-yr data is positioned between the two centers of action of the NAO and extends meridionally toward the centers. The greater area with large standard deviation in Fig. 5a compared to Figs. 5b and 5c arises from the greater variability in a smaller sample size. Generally, the number of grid points with large standard deviation decreases and the meridional extent of large values of standard deviation decreases as the sample size increases, regardless of which year the analysis is centered on in the overlapping periods with different lengths (not shown).

The impact of the length of the time period and of the occasional non-NAO patterns on the NAO uncertainty estimates using 5-yr, 10-yr, and 20-yr data is investigated. It is found that the probability of non-NAO patterns emerging as the leading EOF is very low no matter the length of data. The NAO uncertainty estimate appears to be the same with or without the traditional NAO pattern emerging as the leading EOF.

Our results suggest that NAO uncertainty estimates can be influenced by sampling variability that has the greatest impact for small sample sizes. On the other hand, physical intuition may be revealed by the pattern of NAO uncertainty. Common spatial characteristics of the NAO uncertainty appear to exist in different lengths of data. For example, the maximum standard deviation is located between the two nodes of the NAO, and its location is zonally asymmetric (Fig. 5). Since long records of data are less influenced by sampling variability, we believe that these common spatial characteristics could be physically relevant. To avoid influences from sampling variability, we will focus on the characteristics of the NAO uncertainty based on 20-yr time periods in section 3d.

d. *Characteristics of the NAO uncertainty*

1) MAGNITUDE OF THE NAO UNCERTAINTY

According to Fig. 2, it is noticeable that the magnitude of the standard deviation in the later 20-yr period (1978–97) is smaller than that in the earlier period (1958–77), no matter which method is used. It implies that there is more spatial variability of the NAO in the

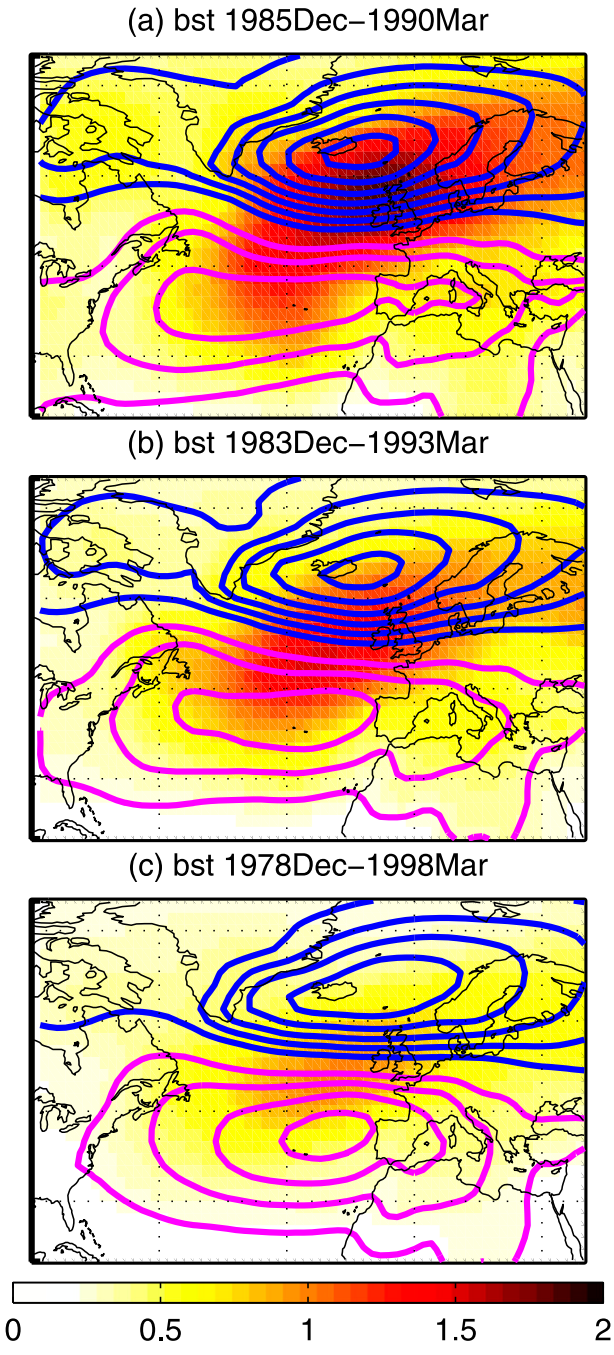

FIG. 5. The NAO (contours) and its standard deviation (shading) estimated by the bootstrap from data based on (a) 5-yr time window centered on 1987, (b) 10-yr window with 1987 as its 5th year, (c) 20-yr window with 1987 as its 10th year. Magenta (blue) contours show positive (negative) values; contour interval is 1 hPa, the zero contour omitted. The scale of the shading is the same in (a)–(c).

earlier period than in the later period. In fact, the magnitude of the NAO uncertainty estimates varies in other 20-yr running windows. Since the NAO uncertainty should be inversely proportional to the variance explained by the NAO, we expect less NAO uncertainty when the pattern is strong (large variance explained or first eigenvalue is relatively large). This statement is supported by the correlation between the time series of maximum standard deviation and that of the variance explained by the NAO over 118 20-yr running windows during 1871–2008, which is about −0.65 with statistical significance.

2) SPATIAL PATTERNS OF THE NAO UNCERTAINTY

Figures 6a and 6b show the NAO (shading), its centers of action (white dots), and its pointwise standard deviation after scaling (thick black contours) for the winters of 1958–77 and 1978–97. In addition to an eastward-located northern node, the NAO pattern in the later period is more longitudinally elongated compared to the earlier period. Furthermore, the corresponding standard deviation patterns of the two periods are different. During 1958–77, the large values of standard deviation are localized between the NAO action centers (Fig. 6a). During 1978–97, the maximum of standard deviation is more longitudinally elongated similar to the corresponding NAO pattern (Fig. 6b).

Figure 6 not only displays the difference in the spatial pattern of standard deviation between the two periods but also addresses their common features. First, both periods have the maximum standard deviation located between the centers of action of the NAO. The results suggest that the NAO uncertainty is dominated by the varying coverages associated with the two nodes of the NAO rather than being influenced by the zonal shift in the NAO. We believe that the location of maximum standard deviation between the two centers of action is associated with the dipole structure of the NAO that has the greatest gradient of the NAO coefficients between the positive and negative NAO centers of action. Because of this unique spatial structure, when the NAO extends or shrinks its coverage, the NAO coefficients located between the centers of action take on different values (positive or negative). In other words, NAO uncertainty is highest close to the zero contour of the NAO pattern. The dominant form of variability of NAO uncertainty is meridional displacements of the zero contour.

Second, the spatial pattern of standard deviation from both periods is not symmetric in the zonal direction. The area of large standard deviation extends in the downstream direction rather than the upstream direction (contours in Figs. 6a,b). Figures 7a and 7b show the mean 300-hPa zonal wind in contours and the standard deviation of the 300-hPa zonal wind anomalies divided by the maximum of standard deviation in shading. The

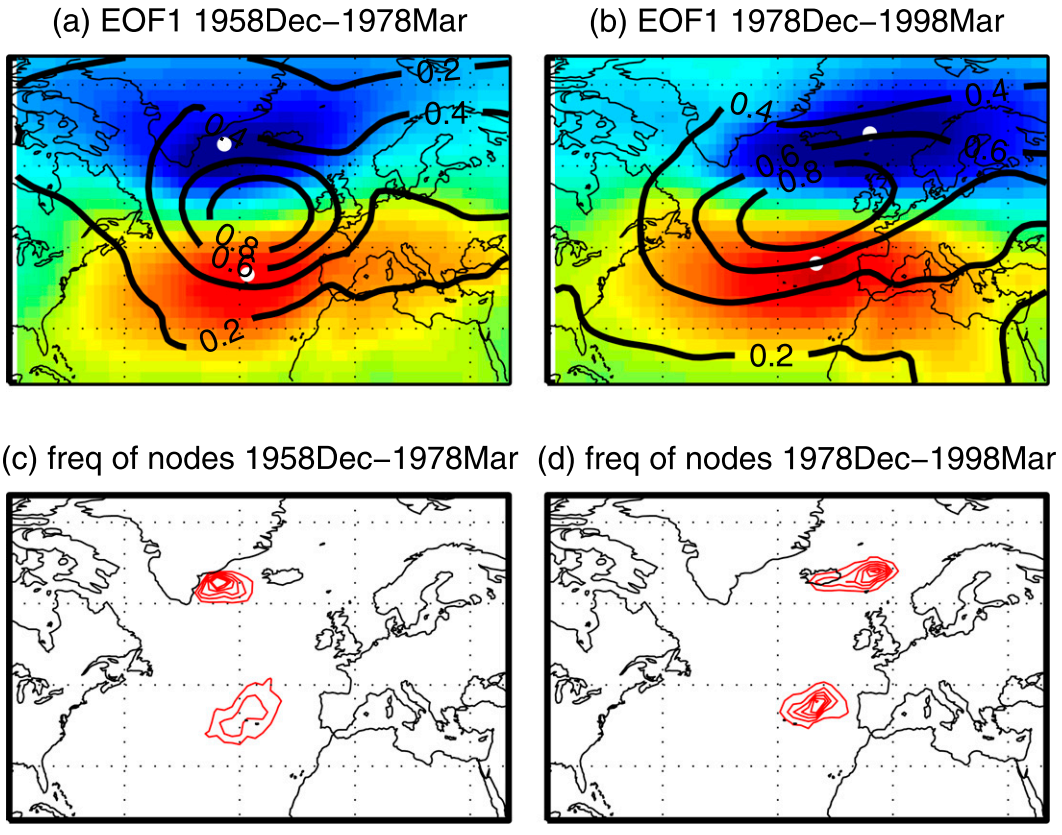

FIG. 6. (top) The NAO (shading), the centers of action (white dots), and standard deviation scaled by the maximum value in each panel (thick black contours) estimated by the bootstrap. (bottom) Red contours show the number of occurrences of the NAO action centers from 1000 bootstrap samples in interval of 20 occurrences. The outermost contour represents 10 occurrences. The periods shown are winters of (left) December 1958–March 1978 and (right) December 1978–March 1998. The scale of contours and shading is the same for each row.

average of the zonal wind component represents the jet and its standard deviation shows the jet variability (Athanasiadis et al. 2010). Scaled standard deviation is shown for the comparison of jet variability between the two periods. Note that the region of large NAO uncertainty overlays the region of large jet variability (cf. contours in Figs. 6a,b to shading in Figs. 7a,b). For both 20-yr periods, the jet core is located over the east coast of the United States while the maximum jet variability meridionally straddles the jet exit region, especially for the earlier period (Fig. 7a).

The key characteristics that we have observed, the maximum of the NAO uncertainty centered between the two nodes of the NAO and the zonal asymmetry, are true for other 20-yr running windows (not shown). The spatial correlation between the NAO uncertainty and jet variability is greater than 0.5 over all 118 20-yr periods, which is statistically significant (the p value is lower than 0.01). The significant spatial correlation supports the close connection between the NAO uncertainty and the jet variability.

e. Distribution of occurrences of NAO action centers

It is intrinsically interesting to look at the variability of location of the NAO action centers. By using the bootstrap technique, we detect the location of the northern and southern nodes of the NAO from each bootstrap sample and count their number of occurrence at each location from 1000 bootstrap samples. In doing so the distribution of occurrences reveals the uncertainty about the locations for the centers of action of the NAO.

Figure 6c and 6d display a 95% confidence region for the location of the NAO nodes (red contours). Specifically, this region contains the most central 950 occurrences out of the 1000 bootstrap samples during the winters of 1958–77 and 1978–97. Generally, the locations of the frequent appearance of the NAO nodes in the bootstrap samples are close to being collocated with the NAO nodes from the original data. Figure 6c and 6d suggest that uncertainty of individual nodes of the NAO in the zonal direction can reach up to 10° longitude. Despite the uncertainty in location of the NAO nodes

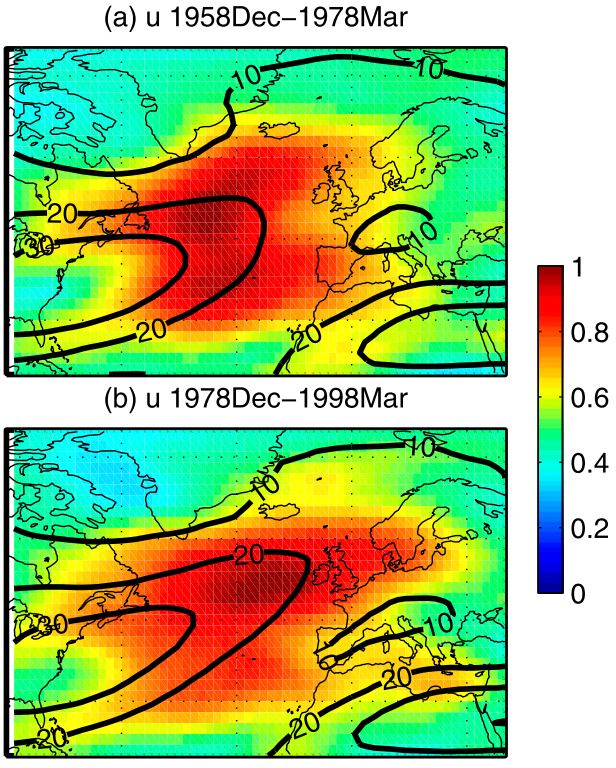

FIG. 7. Mean 300-hPa zonal wind (contours: m s^{-1}) and standard deviation scaled by its maximum (shading) in winters of (a) 1958–77 and 1978–97.

during these two time periods, the boundaries of the confidence regions of the northern node do not overlap. The result implies that, with 95% confidence, the eastward movement of the northern node in the later period is robust and unlikely to be a result of random sampling.

As Wang et al. (2012) indicated in their Fig. 1, the northern and southern nodes are well separated and the temporal variability of longitudes of both NAO action centers is greater than the temporal variability of latitudes. Therefore, we focus on the distribution of longitude of the occurrences of individual NAO action centers and the change in these distributions over time. Figure 8 shows the distribution of the longitude values for the northern (Fig. 8a) and southern nodes (Fig. 8b) over 20-yr running windows for the extent of the twentieth-century analysis. The x axis shows longitude and the y axis shows the 10th year of each 20-yr running window during 1871–2008. If the movement of the NAO action centers between two nonoverlapping time periods is large relative to its uncertainty, we have more confidence in addressing the robustness of the movement. Moreover, Fig. 8 can enhance our understanding of the sudden movement of the NAO action centers between two adjacent periods with overlapping data (Wang et al. 2012).

According to Fig. 8, many of the 20-yr running windows have a well-defined northern node with little uncertainty. Interestingly, the greatest degree of uncertainty of the northern node occurred during the transition between 1958–77 and 1978–97 (note dashed horizontal lines in Fig. 8a), which corresponds to the timing of a sudden eastward movement of the node (yellow curve of Fig. 8a). There are two peaks in the distribution during the transition period, which suggest the possibility of two northern nodes, one located westward around 35°W and another one located eastward around 15°W. The possibility of two northern nodes explains the shift in the late 1970s, which is seen under the assumption of one node. Another noticeable movement occurred in the 1920s and early 1930s. However, its wide uncertainty overlapping with its preceding and following periods in Fig. 8a implies that this movement is not robust.

Generally, the uncertainty of the longitude of the southern node is greater than for the northern node (cf. Fig. 8b to Fig. 8a). The possible reason for this greater uncertainty is that the southern node may appear in more than two different locations. Large uncertainty in the location of the southern node occurred in particular before 1920. Three southern nodes appeared to be located near 35°W, 15°W, and 10°E in the late nineteenth century. As time passed, the southern node began to be well defined and located westward in the 1920s. Then it shifted to the east in the 1940s and shifted back to the west in the 1960s. Similar to its northern counterpart, the uncertainty in the longitude of the southern node during the 1950s covers two separate longitudinal ranges suggesting the possibility of two southern nodes, which may be influenced by its preceding and following periods (cf. dashed lines in Fig. 8b).

4. Discussion and conclusions

This study measures the uncertainty of the EOF-defined North Atlantic Oscillation, which is not provided by traditional EOF analysis. We use both parametric and nonparametric methods. Using the asymptotic approximation, we are constrained by the underlying assumption of normally distributed data. The bootstrap does not have this constraint, and the discrepancy between the bootstrap and the asymptotic approximation decreases as sample size increases. The results suggest that the difference in uncertainty estimates between the asymptotic and bootstrap approaches is due to a combination of sample size and the lack of normality of data. Generally, the bootstrap offers plausible measures of the NAO uncertainty that is both relevant to statistical issues (e.g., sampling variability) and physical issues

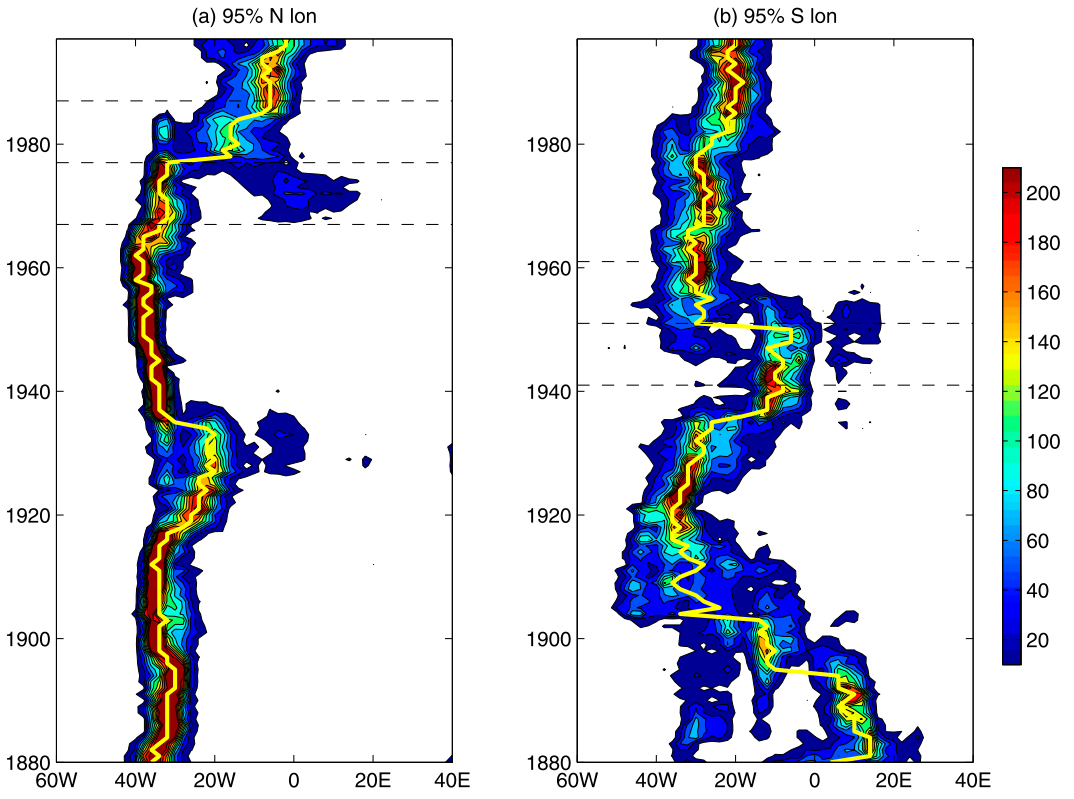

FIG. 8. Distribution of the longitude of occurrence of individual NAO nodes vs 20-yr running windows: (a) the northern node and (b) the southern node. Yellow curve shows longitude of centers of action from the estimation in original data. The *y* axis shows the 10th year of a 20-yr period. The dashed lines in (a) from bottom to top mark the 20-yr periods with 1967, 1977, and 1987 as the 10th year. The dashed lines in (b) from bottom to top mark the 20-yr periods with 1941, 1951, and 1961 as the 10th year.

(e.g., jet variability). As expected, sampling variability plays a larger role in the NAO uncertainty for shorter records of data. As the sample size increases, the magnitude of NAO uncertainty decreases and its pattern is more confined between the centers of action of the NAO. Since NAO uncertainty is dependent on sample size, using a longer record of data can lower the fraction of NAO uncertainty resulting from sampling variability and shed more light on the connection between the NAO spatial variability and physical mechanisms.

There are common features of the NAO uncertainty that are of interest. For instance, large values of standard deviation are located between the centers of action of the NAO where the largest gradient of the NAO coefficients is located owing to its dipole structure. The result suggests that NAO uncertainty is dominated by varying spatial extent of the NAO rather than the zonal shift in the centers of action of the NAO. Moreover, the NAO uncertainty is zonally asymmetric and its maximum values overlay the regions of large jet variability downstream of the jet maximum. There is an interesting connection between NAO uncertainty and jet variability. Jet variability is associated with two leading modes, pulsing and wobbling of the jet. Pulsing is associated with variability in jet strength, whereas wobbling is associated with a shift in jet location. These two modes appear to correspond to the two types of NAO uncertainty, due to 1) varying spatial coverage between the centers of action and 2) a zonal shift in the NAO, respectively. The 20-yr period 1978–97 was characterized by more spatial variability due to pulsing of the jet or uncertainty of the NAO due to changing coverage of the NAO centers of action, whereas the 20-yr period 1958–77 was characterized by the wobbling jet.

In addition to the comparison of the spatial patterns of the NAO uncertainty between two periods, an intuitive interpretation to assess the shift in the NAO between two periods is to compare their distribution of location of NAO action centers. If the 95% confidence regions of the distribution of the NAO nodes of two periods do not overlap, we have more confidence in addressing the robustness of the shift. Multiple local maxima seen in the distribution of location reveal the possibility of multiple centers. A greater possibility of multiple centers often

occurs as a well-defined action center transfers from one location to another such as occurred in the late 1970s (see Fig. 8a).

Since the National Centers for Environmental Prediction (NCEP)–National Center for Atmospheric Research reanalysis data are constrained by observations in the free atmosphere as well as surface observations, we examine NAO uncertainty in 1958–77 and 1978–97 using the NCEP monthly mean data using the same bootstrap techniques used for 20CRv2. We find that the spatial pattern and magnitude of NAO uncertainty using the NCEP data are almost identical to that using the 20CRv2. The significance of the shift in the 1978–97 compared to 1958–77 is confirmed again. The consistency of NAO uncertainty between the two datasets, as well as other independent data such as sea ice export (Hilmer and Jung 2000), implies the robustness of the shift in the NAO.

Given that NAO variability covers a wide range of time scales, NAO uncertainty may alternate as different frequency bounds are included in the data. Since monthly mean data filter out the high-frequency synoptic signal, it is of interest to examine NAO uncertainty using weekly mean data. Weekly data are calculated by averaging consecutive seven days from 1 December to early April (4 April for leap years and 5 April for normal years). Thus, there are 18 weeks each winter and 360 weeks for a 20-yr period. The weekly anomalies are derived by subtracting the 20-yr average of weekly data for the relevant week. We apply the bootstrap to the weekly anomalies and obtain NAO uncertainty. NAO uncertainty estimated by the bootstrap using weekly data has a similar spatial pattern to that obtained by the bootstrap using monthly data (not shown). NAO patterns resulting from weekly data have maximum NAO uncertainty embedded between the NAO action centers similar to the analysis of monthly data. However, differences in NAO uncertainty between monthly data and weekly data can be detected. Analysis resulting from weekly data is generally noisier than analysis resulting from monthly data. For example, the eastward shift in the northern node of the NAO for the 20-yr period 1978–97 compared to 1958–77 is less robust in weekly data, but the shift is still present.

Acknowledgments. This work is supported by NSF Grant AGS-1025374. We thank Dr. Adam Monahan and two anonymous reviewers for helpful comments on the manuscript.

REFERENCES

Athanasiadis, P. J., J. M. Wallace, and J. J. Wettstein, 2010: Patterns of wintertime jet stream variability and their relation to the storm tracks. *J. Atmos. Sci.,* **67,** 1361–1381.

Cassou, C., L. Terray, J. W. Hurrell, and C. Deser, 2004: North Atlantic winter climate regimes: Spatial asymmetry, stationarity with time, and oceanic forcing. *J. Climate,* **17,** 1055–1068.

Compo, G. P., and Coauthors, 2011: The Twentieth Century Reanalysis Project. *Quart. J. Roy. Meteor. Soc.,* **137,** 1–28, doi:10.1002/qj.776.

Efron, J., and R. J. Tibshirani, 1994: *An Introduction to the Bootstrap.* 1st ed. Chapman and Hall/CRC, 465 pp.

Gentle, J., W. Hardle, and W. Mori, 2004: *Handbook of Computational Statistics.* 1st ed. Springer, 900 pp.

Hannachi, A., I. T. Jolliffe, and D. B. Stephenson, 2007: Empirical orthogonal functions and related techniques in atmospheric science: A review. *Int. J. Climatol.,* **27,** 1119–1152.

Hilmer, M., and T. Jung, 2000: Evidence for a recent change in the link between the North Atlantic Oscillation and Arctic sea ice export. *Geophys. Res. Lett.,* **27,** 989–992.

Hurrell, J. W., 1995: Decadal trends in the North Atlantic Oscillation: Regional temperatures and precipitation. *Science,* **269,** 676–679.

Jolliffe, I. T., 2002: *Principal Component Analysis.* 2nd ed. Springer, 502 pp.

Kunsch, H. R., 1989: The jackknife and the bootstrap for general stationary observations. *Ann. Stat.,* **17,** 1217–1241.

North, G. R., T. L. Bell, R. F. Cahalan, and F. J. Moeng, 1982: Sampling errors in the estimation of empirical orthogonal functions. *Mon. Wea. Rev.,* **110,** 699–706.

Peng, S. L., and J. Fyfe, 1996: The coupled patterns between sea level pressure and sea surface temperature in the midlatitude North Atlantic. *J. Climate,* **9,** 1824–1839.

Quadrelli, R., C. S. Bretherton, and J. M. Wallace, 2005: On sampling errors in empirical orthogonal functions. *J. Climate,* **18,** 3704–3710.

Seber, G. A. F., 1984: *Multivariate Observations.* 1st ed. Wiley, 686 pp.

Venegas, S. A., L. A. Mysak, and D. N. Straub, 1997: Atmosphere–ocean coupled variability in the South Atlantic. *J. Climate,* **10,** 2904–2920.

von Storch, H., and F. W. Zwiers, 1999: *Statistical Analysis in Climate Research.* 1st ed. Cambridge University Press, 484 pp.

Wallace, J. M., and D. S. Gutzler, 1981: Teleconnections in the geopotential height field during the Northern Hemisphere winter. *Mon. Wea. Rev.,* **109,** 784–812.

Wang, Y.-H., and G. Magnusdottir, 2012: The shift of the northern node of the NAO and cyclonic Rossby wave breaking. *J. Climate,* **25,** 7973–7982.

——, ——, H. Stern, X. Tian, and Y. Yu, 2012: Decadal variability of the NAO: Introducing an augmented NAO index. *Geophys. Res. Lett.,* **39,** L21702, doi:10.1029/2012GL053413.

Wilks, D. S., 1997: Resampling hypothesis tests for autocorrelated fields. *J. Climate,* **10,** 65–82.

Zhang, X., A. Sorteberg, J. Zhang, R. Gerdes, and J. C. Comiso, 2008: Recent radical shifts of atmospheric circulations and rapid changes in Arctic climate system. *Geophys. Res. Lett.,* **35,** L22701, doi:10.1029/2008GL035607.